Fission dynamics of intermediate-fissility systems: A study within a stochastic three-dimensional approach

E. Vardaci,* P. N. Nadtochy,† A. Di Nitto,‡ A. Brondi, G. La Rana, R. Moro, P. K. Rath, and M. Ashaduzzaman
Dipartimento di Fisica, Universitá degli Studi di Napoli "Federico II" and Istituto Nazionale di Fisica Nucleare, Sezione di Napoli, 80126 Napoli, Italy

E. M. Kozulin, G. N. Knyazheva, and I. M. Itkis
Flerov Laboratory of Nuclear Reaction, Joint Institute for Nuclear Research, 141980 Dubna, Moscow Region, Russia

M. Cinausero and G. Prete
Laboratori Nazionali di Legnaro dell'Istituto Nazionale di Fisica Nucleare, 35020 Legnaro (Padova), Italy

D. Fabris and G. Montagnoli
Istituto Nazionale di Fisica Nucleare and Dipartimento di Fisica, 35131 Padova, Italy

N. Gelli
Istituto Nazionale di Fisica Nucleare, Sezione di Firenze, 50019 Firenze, Italy

The system of intermediate fissility ^{132}Ce has been studied experimentally and theoretically to investigate the dissipation properties of nuclear matter. Cross sections of fusion-fission and evaporation-residue channels together with light charged particle multiplicities in both channels, their spectra, light charged particle-evaporation residue angular correlations, and mass-energy distribution of fission fragments have been measured. Theoretical analysis has been performed using a multidimensional stochastic approach coupled with a Hauser-Feshbach treatment of particle evaporation. The main conclusions are that the full one-body shape-dependent dissipation mechanism allows the reproduction of the full set of experimental data and that after a time $\tau_d = 5 \times 10^{-21}$ s from the equilibrium configuration of the compound nucleus, fission decay can occur in a time that can span several orders of magnitude.

I. INTRODUCTION

The dissipation properties of nuclear matter are a substantial subject in experimental and theoretical investigations with heavy-ion reactions. Nuclear friction that accompanies the fission process is expected to reduce the Bohr-Wheeler fission rate and to cause a stationary value to be reached only after a delay. During the past decades many efforts have been undertaken to get a precise determination of the fission time scale, the nature of dissipation, and the dependence of dissipation on the temperature and deformation. Whether nuclear dissipation proceeds primarily by means of individual two-body collisions (two-body friction), as the case of an ordinary fluid, or by means of nucleons colliding with a moving potential wall (one-body friction) is still a matter of debate. The estimations given by different authors predict quite a wide range of dissipation strength and possible dependencies on temperature and deformation (see review [1] and references therein [2,3]). The lack of constraints to the model appears to be, in several cases, one of the source of controversies because the theoretical predictions depend on many parameters and models, such as level density, transmission coefficients [4,5], and dimensionality of the model [6,7], and not only on the friction coefficient. Consequently, the comparison between a large number of observables with the ones calculated from a unified theoretical model could provide more severe constraints on the parameter values involved in a nuclear dissipation model. Therefore, one needs to use an elaborated theoretical model that realistically treats all the possible decay channels and computes the many measured observables.

II. FISSION IN SYSTEMS OF INTERMEDIATE FISSILITY

It was already pointed out in Refs. [8,9] that systems of intermediate fissility ($A \approx 100$–180, $\chi \approx 0.5$–0.6) are very little studied, although they offer several advantages. For instance, (1) they are characterized by an evaporation-residue (ER) cross section comparable to or larger than the fusion-fission (FF) cross section; (2) they have also much larger light-charged-particle (LCP) multiplicities, which could be investigated together with neutrons; and (3) the potential energy surface is characterized by a shorter path from the saddle to the scission point.

The first point implies that the predictions of the theoretical models can be constrained not only by observables in the FF

*Corresponding author: Emanuele.Vardaci@na.infn.it
†Present address: Omsk State University, Mira prospekt 55-A, 644077 Omsk, Russia.
‡Present address: Johannes Gutenberg-Universität Mainz, 55099 Mainz, Germany.

channel but also by observables relative to the ER channel, such as particle multiplicities, their spectra, and angular correlations. The second point implies that the effects of the fission delay over the FF and ER cross sections is much more pronounced because the emission of a charged particle in the presaddle region strongly enhances the probability of producing an ER as a consequence of both a reduction of the excitation energy and fissility. This correlation induced by the nuclear viscosity between the enhanced yield of pre-scission particles and the survival of ERs might be an important channel for the feeding of ERs having large deformations in the mass region of $A \approx 150$–160 [10]. Therefore, the measurements of the relevant quantities in both FF and ER channels make it possible to add more severe constraints on the model predictions.

Finally, the third point implies that saddle and scission configurations are relatively close in the deformation space and, therefore, the role of the presaddle dynamics relative to the saddle-to-scission dynamics is enhanced. Consequently, some of the ambiguities on the not-well-identified separation and interplay between pre- and postsaddle dynamics is less effective in the interpretation of the data.

In the present paper we report the results of theoretical calculations compared with experimental data for the reaction 200 MeV ^{32}S + ^{100}Mo. We have measured most of the relevant quantities in the ER and FF channels: proton and α-particle energy spectra and multiplicities, ER and FF cross sections, as well as mass and total-kinetic-energy distributions of fission fragments. The extraction procedure of the proton and α-particle multiplicities from the energy spectra measured in coincidence with ER and FF is the same as in Refs. [11] and [5,12], respectively. Theoretical modeling of the fission process has been performed using a three-dimensional dynamical model [13–15] based on the Langevin equations coupled with the statistical description of light-particle evaporation. This model allows to investigate the parameters of the fission-fragment mass-energy distribution (MED), as well as the different characteristics of the evaporated particles in FF and ER channels.

The main goal of this work is to explore some debated aspects of the fission process: the fission time scale, the nature and the strength of the nuclear viscosity and its possible dependence on the nuclear shape, and the temperature. Fission dynamics is studied consistently from the ground state of the compound nucleus to its scission under discrete cooling owing to the evaporation of particles. The mean particle multiplicities in the ER and FF channels, their spectra and angular correlations, as well as the parameters of the two-dimensional MED of fission fragments are investigated. We intend to draw some conclusions about the dissipation mechanism of nuclear collective motion in fission of excited nuclei by comparison of the theoretically calculated values with the experimental data. The most important point of our study is the attempt to describe self-consistently a large number of experimental observables in FF and ER channels with a unique set of input parameter values and only varying the type and strength of nuclear dissipation.

The article is organized as it follows. In Sec. I, we review the available experimental data [4,5] and describe in detail the experimental data that we are going to add to the set of data to be compared to the dynamical theoretical model. In Sec. II, we describe the theoretical model in some detail. In Sec. III we discuss the result of the comparison and in Sec. IV we draw our conclusions.

III. EXPERIMENTAL SETUPS AND OBSERVABLES

In this section we review the experimental setups used and the measured observables. A detailed description of the setups and methods used to extract the observables is provided in Refs. [4,5]. However, we describe in some detail the extraction of some new observables not used in the analysis performed earlier [4,5] and that will be used in the present work to enlarge even more the set of observables.

We used three different setups, 8πLP [16], PISOLO [17], and CORSET [18], in three different experiments performed at the XTU Tandem-ALPI Superconducting LINAC accelerator complex of the Laboratori Nazionali di Legnaro (LNL), Legnaro, Italy.

To favor an easy reading, all the obtained experimental data are reported in Sec. V (Results and Discussion) in conjunction with the results of the dynamical model calculations. In this section we describe the detectors and the techniques used to extract the many observables.

A. FF, ER, and light-charged-particle detection

Multiplicities, energy spectra, and angular distributions of LCPs in the FF and ER channels were measured with the BALL sector of the 8πLP apparatus. A schematic layout of the setup is given in Fig. 1(a). The experiment was performed at the XTU Tandem-ALPI Superconducting LINAC accelerator complex. A 200-MeV pulsed beam (with period of 800 ns and

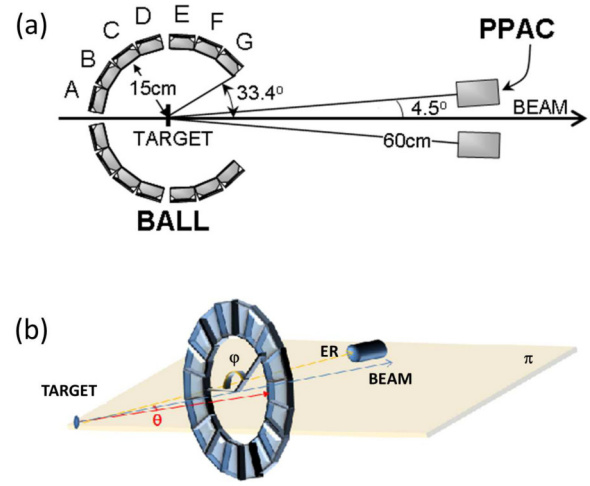

FIG. 1. (Color online) (a) Schematic layout of the experimental apparatus. The letters from A to G label the seven rings of the BALL section. (b) The geometry used for the angular distribution of LCP detected in a ring around the beam in coincidence with ER detected in a parallel-plate avalanche counter (PPAC) horizontal plane. π indicates the reaction plane, which is defined as the plane containing the beam and the PPAC.

duration of about 3 ns) of ^{32}S of about 1–3 enA intensity was used to bombard a self-supporting ^{100}Mo target, 400 μg/cm^2 thick.

In 8πLP particle identification is carried out by the ΔE-E method in Si-CsI telescopes and, for particles stopping in the first stage of the telescope, by the pulse-shape-discrimination (PSD) technique as the silicon detectors are mounted with the rear side facing the target, in the so-called *flipped* configuration. With this kind of telescope it is possible to measure energies up to 34 A MeV with energy thresholds of 0.5 MeV for protons and 2 MeV for α particles.

To detect ERs the 8πLP setup is equipped with four parallel-plate avalanche counter (PPAC) modules. Two PPACs are mounted in the vertical plane and two on the horizontal plane, each of them at 4.5° with respect to the beam direction [Fig. 1(a)]. By using the time-of-flight (TOF) technique it is possible to separate fast fragments (typically elastic scattering or fission fragments) from the slower ones, namely the ERs. The symmetrical positioning of the PPAC is very useful because one can benefit from the spherical symmetry of the BALL. Each direction of the PPAC defines, along with the beam direction, a reaction plane π [Fig. 1(b)] in the ER channel. Each reaction plane selects a direction of the spin of the compound nucleus (orthogonal to the reaction plane) with some disalignments owing to particle evaporation (considered later in the simulations). For each reaction plane (namely, for each spin direction) an extended in-plane and out-of-plane distribution can be measured by choosing the detectors of a ring whose azimuthal angle φ ranges from 0 to 2π and whose polar angle is fixed by the ring chosen between A and G (see Fig. 1). In this way it is possible to highlight the effect of the spin on the angular distribution, and the different kinematical kick and event rates when the LCP is observed on the opposite side of the PPAC (higher rate) or on the same side (lower rate) with respect to the beam. Furthermore, the coincidence events between the BALL and each PPAC can be summed correspondingly to improve the statistics.

In a separate experiment ER cross section was measured by means of PISOLO [17], the electrostatic deflector of LNL. A more detailed description of the methods and details used in the experiment are given in Ref. [5].

Heavy fragments from two-body reactions were detected in double-coincidence mode in the telescopes of the most forward rings of the BALL which cover the angles from 33° to 70° [rings F and G of Fig. 1(a)]. Because these fragments do not cross the first stage of the telescope, the PSD technique was used to discriminate between the heavy fragments and the LCP stopping in the ΔE detector of the same telescope. Details are given in Ref. [5].

B. Mass-energy distribution of the fission fragments and FF cross section

The measurement of mass and total-kinetic-energy (TKE) distribution of the fission fragments has been carried out at LNL using the TOF spectrometer CORSET [18]. A double-arm TOF spectrometer, with a flight path of 30 cm, forms the basis for the experimental setup. This spectrometer includes a compact START microchannel plate (MCP) detector and a position-sensitive MCP STOP detector. The two arms replace two telescopes of the ring F on the opposite side with respect to the beam. The raw quantities measured are the time spent by the ion to span the flight path (distance between start and stop detectors) and the (x, y) position of the impact point on the stop detector. These three raw quantities, measured in coincidence for both fragments, allow the estimation the primary mass and energy of the fragments if the two-body kinematics equations are employed.

The time resolution of CORSET is of the order of 150 ps. This feature makes it possible to achieve a mass resolution of ≈ 2 mass units. From the raw fission-fragment data, we can determine, for each fragment, the velocity vectors, $\vec{v}_1$ and $\vec{v}_2$, and the primary masses, M_1 and M_2. The primary mass refers to the mass of a fragment at scission point. The procedure includes several corrections and is based on a successive approximation method. In the zero approximation, fragment velocity vectors $\vec{v}_1^0$ and $\vec{v}_2^0$ are determined from the TOF and from the registered coordinates. The main source of errors at this stage comes from the unaccounted energy loss in the START detector converter foil and in the target (in both cases energy loss is $\approx$5 MeV for each fragment in a symmetrical mass split). The first approximation for fragment masses $M_{1,2}^0$ is calculated using momentum conservation perpendicular to the beam axis $M_1^0 v_1^{0\perp} = M_2^0 v_2^{0\perp}$ and assuming that the two fragment masses add up to the mass of the compound system prior to fission, $M_1^0 + M_2^0 = M_{\text{projectile}} + M_{\text{target}} - \langle M^{\text{pre}} \rangle$, where $\langle M^{\text{pre}} \rangle$ is the mean total mass of particles evaporated from the compound nucleus before scission. Because, according to our model predictions, neutrons dominate the pre-scission emission, $\langle M^{\text{pre}} \rangle$ was assumed to be equal to neutron pre-scission multiplicity $\langle M_n^{\text{pre}} \rangle$. The value of $\langle M_n^{\text{pre}} \rangle$ was taken from systematics [19]. The influence of uncertainty in $\langle M^{\text{pre}} \rangle$ determination turned out to be much smaller than the overall errors. From $\vec{v}_{1,2}^0$ and $M_{1,2}^0$ fragment energies $E_{1,2}^0$ are determined using nonrelativistic formulas. The known fragment mass and energy allows us to calculate consequently the energy lost in the START detector and the target. From the corrected values of $E_{1,2}^1 = E_{1,2}^0 + \Delta E^{\text{START}} + \Delta E^{\text{target}}$ and old values of fragment masses $M_{1,2}^0$, new values of the fragment velocities in the target are calculated. The above procedure is repeated until it converges, namely, when the last values of the masses obtained is within 1 or 2 mass units from the ones calculated in the step before last. Usually, fewer than ten iterations are sufficient. Using the extracted values of $\vec{v}_{1,2}$ and $M_{1,2}$ the MED of fission fragments $Y(M, E_K)$ are calculated. The one-dimensional mass and kinetic-energy distributions of fission fragments are obtained by the integration of $Y(M, E_K)$ over kinetic energy or mass, respectively.

In a third experiment, the angular distribution of the fission fragments was measured with a TOF-E spectrometer based on CORSET. The spectrometer consists in this case of a single arm that can be rotated around the target and that allows the simultaneous measurement of the velocity (via the TOF) and the energy of a fragment [5]. The arm was positioned at six laboratory angles between 14° and 50°. The differential cross section was obtained by proper normalization to elastic scattering and then angle integrated to obtain the fission cross section.

IV. DYNAMICAL APPROACH

In this section we describe the dynamical model used to extract features of the fission process. The starting point is the dynamical model developed in Refs. [13,14]. This model has been further extended to improve the evaporation of light particles (n,p,α) during the fission process and include the evaporation from ER if formed.

A. Dynamical model and dissipation

In all the dynamical approaches, a limited set of collective variables must be chosen. Usually, most of them concern the shape of the nucleus en route toward fission. In the dynamical model in Refs. [13,14] a (c,h,α) parametrization [20] of the nuclear shape is applied. The surface of the nucleus in cylindrical coordinates is given by

$$\rho_s^2(z) = \begin{cases} (c^2 - z^2)\left(A_s + Bz^2/c^2 + \frac{\alpha z}{c}\right), & B \geqslant 0, \\ (c^2 - z^2)\left(A_s + \frac{\alpha z}{c}\right)\exp(Bcz^2), & B < 0, \end{cases} \quad (1)$$

where z is the coordinate along the symmetry axis and ρ_s is the radial coordinate of the nuclear surface. In Eq. (1) the quantities B and A_s are defined as

$$B = 2h + \frac{c-1}{2},$$

$$A_s = \begin{cases} c^{-3} - \frac{B}{5}, & B \geqslant 0, \\ -\frac{4}{3}\frac{B}{\exp(Bc^3) + \left(1+\frac{1}{2Bc^3}\right)\sqrt{-\pi Bc^3}\,\mathrm{erf}(\sqrt{-Bc^3})}, & B < 0. \end{cases} \quad (2)$$

In Eqs. (1) and (2), c denotes the elongation parameter, the parameter h describes the variation in the thickness of the neck for a given elongation of the nucleus, and the parameter of the mass asymmetry α determines the ratio of the volumes of the future fission fragments.

In the stochastic approach [21–24] evolution of the collective coordinates is considered as motion of Brownian particles which interact stochastically with a large number of internal degrees of freedom, constituting the surrounding heat bath. The friction force is assumed to be derived from the random force averaged over a time larger than the collisional time scale between collective and internal degrees of freedom. The random part is modeled as a Gaussian white noise that causes fluctuations of the collective variables, and, as a result, fluctuations of the physical observables in fission process. The coupled Langevin equations have the form

$$\frac{dq_i}{dt} = \mu_{ij} p_j,$$

$$\frac{dp_i}{dt} = -\frac{1}{2} p_j p_k \frac{\partial \mu_{jk}}{\partial q_i} - \frac{\partial F}{\partial q_i} - \gamma_{ij}\mu_{jk} p_k + \theta_{ij}\xi_j(t), \quad (3)$$

where $\mathbf{q}$ is the vector of collective coordinates, $\mathbf{p}$ is the vector of conjugate momenta, $F(\mathbf{q}) = V(\mathbf{q}) - a(\mathbf{q})T^2$ is the Helmholtz free energy, $V(\mathbf{q})$ is the potential energy, $m_{ij}(\mathbf{q})$ $(\|\mu_{ij}\| = \|m_{ij}\|^{-1})$ is the tensor of inertia, $\gamma_{ij}(\mathbf{q})$ is the friction tensor. The normalized random variable $\xi_j(t)$ is assumed to be a white noise. The strength of the random force θ_{ij} is given by Einstein relation $\sum \theta_{ik}\theta_{kj} = T\gamma_{ij}$. The temperature of the "heat bath" T has been determined by the Fermi-gas model formula $T = (E_{\mathrm{int}}/a)^{1/2}$, where E_{int} is the internal excitation energy of the nucleus and a is the level-density parameter. The repeated indices in the equations above imply summation over the collective coordinates.

The collective coordinates $\mathbf{q} = (q_1,q_2,q_3)$ are connected with the shape parameters c,h, and α by $q_1 = c$, $q_2 = (h + 3/2)/(\frac{5}{2c^3} + \frac{1-c}{4} + 3/2)$, and $q_3 = \alpha/(A_s + B)$, if $B \geqslant 0$, or $q_3 = \alpha/A_s$, if $B < 0$. The advantage of using the collective coordinates $\mathbf{q}$ instead of the (c,h,α) parameters is discussed in Refs. [25,26].

During a random walk along a Langevin trajectory in the collective coordinates space, the energy conservation law is used in the form $E_x(t) = E_{\mathrm{int}} + E_{\mathrm{coll}} + V + E_{\mathrm{evap}}(t)$. Here E_x is the total excitation energy of the nucleus, $E_{\mathrm{coll}} = 0.5\sum \mu_{ij} p_i p_j$ is the kinetic energy of the collective degrees of freedom. The value $E_{\mathrm{evap}}(t)$ is the energy carried away by the evaporated particles at the time t. The inertia tensor is calculated by means of the Werner-Wheeler approximation for incompressible irrotational flow [27]. The potential energy of the nucleus is calculated within the framework of a macroscopic model with finite range of the nuclear forces [28] with parameters from Ref. [29].

One-body [30,31] and two-body [27] mechanisms of nuclear dissipation have been used for the determination of the dissipative part of the driving force in the present analysis. We used a modified version of the one-body mechanism with a reduction coefficient of the contribution from the wall formula k_s [32,33]. The value $k_s = 1.0$ corresponds to the wall and wall-plus-window formulas [30], whereas values $0.2 < k_s < 0.5$ make it possible to reproduce different characteristics of the MED and particle multiplicities [13,14,25] and are compatible with other predictions [34–37].

For strongly necked-in shapes the friction tensor is calculated using the wall-plus-window formula. For compact mononuclear shapes only the wall formula is used with the reduction factor k_s. In the intermediate case for the shapes which are neither compact nor strongly necked in, a smooth interpolation [38,39] between the wall and the wall-plus-window formulas has been used, with a form factor going to 1 for mononuclearlike shapes, and going to 0 for the shapes with zero neck radius. The present calculations have been performed with the k_s values ranging from 0.1 to 1.0.

To explore the possibility to reproduce the full set of experimental data, we performed calculations with the two-body dissipation mechanism [27] as well. We have varied the two-body dissipation coefficient ν_0 from 0.02×10^{-21} MeV s fm^{-3} to 0.5×10^{-21} MeV s fm^{-3}. The first value of ν_0 is slightly larger than the values used in Refs. [40,41] in their dynamical calculations, where only the mean kinetic energy of fission fragments $\langle E_K \rangle$ was investigated. The larger value $\nu_0 = 0.5 \times 10^{-21}$ MeV s fm^{-3} is close to the one used in the study of Wada *et al.* [42] to reproduce only the neutron pre-scission multiplicity and cross sections of FF and ER channels in the fission of ^{200}Pb. We underline here that in Ref. [42] fission-fragment kinetic energy and neutron pre-scission multiplicity could not be reproduced with the same value of the parameter ν_0.

Usually the analysis of dissipation properties of nuclear matter is performed using the reduced dissipation coefficient

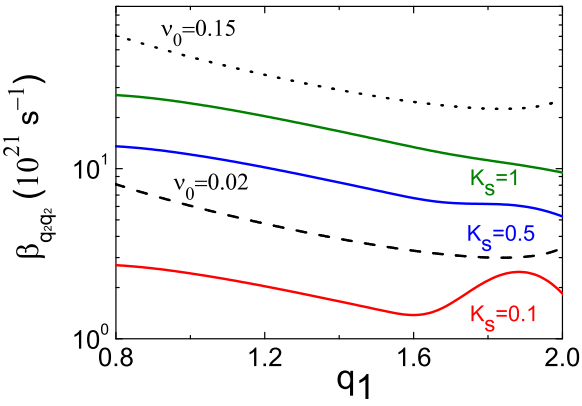

FIG. 2. (Color online) The reduced friction coefficient $\beta_{q_2q_2}$ as a function of elongation for ^{132}Ce composite system for the one-body dissipation mechanism with the values of reduction coefficient from the wall formula $k_s = 1$, 0.5, and 0.1 and for two-body dissipation mechanism with the the two-body dissipation coefficient $\nu_0 = 0.02 \times 10^{-21}$ MeV s fm^{-3} and $\nu_0 = 0.15 \times 10^{-21}$ MeV s fm^{-3}.

$\beta = \gamma/m$. In the typical statistical model approach to fission dynamics this coefficient is used as a fixed parameter. In our model it is calculated as $\beta_{q_2q_2} = \gamma_{q_2q_2}/m_{q_2q_2}$, namely, as a ratio of components of the friction $\gamma_{q_2q_2}$ and mass $M_{q_2q_2}$ tensors. For this reason, $\beta_{q_2q_2}$ is shape dependent, in both one- and two-body dissipation, and determines the overdamped or underdamped character of the motion along the elongation coordinate from spherical shape to the scission deformation. The trend of the friction coefficient $\beta_{q_2q_2} = \gamma_{q_2q_2}/m_{q_2q_2}$ as a function of the nuclear elongation along the bottom of the fission valley is shown in Fig. 2 for different values of one-body reduction factor k_s and for different values of the two-body dissipation coefficient ν_0.

Assuming full one-body dissipation ($k_s = 1$), we observe a strong dependence of $\beta_{q_2q_2}$ on deformation; namely, dissipation is smaller for more elongated shapes. Large values of $\beta_{q_2q_2} \simeq 24 \times 10^{21}$ s^{-1} are involved in compact shapes near spherical deformation ($q_1 = 1$) at the beginning of the fission process. A decreasing behavior of $\beta_{q_2q_2}$ is observed with the increase of deformation. The dependence on nuclear deformation becomes weaker for smaller values of k_s. Of interest is the bump in $\beta_{q_2q_2}$ toward the scission point for the case of a weaker one-body dissipation ($k_s = 0.1$). This behavior may recall what is expected in the statistical model approach to fission dynamics where more intense dissipation in the saddle-to-scission motion, with respect to presaddle, is necessary to reproduce the neutron pre-scission multiplicities [1]. However, as shown in the next section, this case does not make it possible to reproduce the full set of data of the system under exam within the dynamical approach.

Concerning two-body dissipation, by adopting the standard intensity given by $\nu_0 = 0.02 \times 10^{-21}$ MeV s fm^{-3} one gets a smooth decrease of $\beta_{q_2q_2}$ from the values $\beta_{q_2q_2} \simeq 7 \times 10^{21}$ s^{-1} to $\beta_{q_2q_2} \simeq 3 \times 10^{21}$ s^{-1} at the scission deformation. The increase of the parameter ν_0 results in an increase of $\beta_{q_2q_2}$, keeping the same deformation dependence of $\beta_{q_2q_2}$ on elongation at logarithmic scale. In the present calculations the friction tensor is assumed to be independent from the temperature in one-body as well as two-body dissipation mechanisms.

B. Evaporation of light particles along a trajectory

In the motion toward fission, the composite system may evaporate light particles. Evaporation of light particles is incorporated into the present model and makes it possible to compute not only multiplicities, but also particle energy spectra in the ER channel and, in particular, in the pre-scission channel. It is important to remark that this latter is a new and important feature of the present model code which is not anymore limited at the calculation of the pre-scission multiplicities alone. This means that the pre-scission particle energy spectra can now provide important inputs into the description of the fission process and can be used to further constrain the model. For instance, one of the advantages of the present implementation is that the shape of the nucleus is known at each time step and the evaporation probability can take advantage of this information which is not experimentally accessible. Furthermore, the evaporation along a trajectory may change the destiny of a composite system, which may not be anymore in the condition to fission.

During the time evolution of a trajectory the internal excitation energy is calculated at each time step. The partial evaporation widths $\Gamma_j (j = n, p, \alpha)$ are calculated using the statistical model LILITA_N97 [43]. The detailed description of the model can be found in Ref. [5]. For the calculations of the Γ_j the transmission coefficients are taken from fusion systematics [44] and the level density is the well-known Fermi-gas model formula. The Langevin equations are integrated by means of the Heuen finite difference scheme [23,45] of the first order with the step of integration Δt. Knowing the time step of the difference scheme we can determine the probability for the nucleus to evaporate a particle using the following procedure [46]: A random number ζ uniformly distributed in the interval (0,1) is generated and compared with the ratio of the time step Δt to the mean evaporation time $\tau_{\rm tot} = \hbar/\Gamma_{\rm tot}$, where $\Gamma_{\rm tot} = \sum_j \Gamma_j$. It is assumed that one of the particles (n, p, α) is evaporated if $\zeta < \frac{\Delta t}{\tau_{\rm tot}}$. A specific particle is chosen by means of Monte Carlo sampling; namely, the probability of emitting a given particle is proportional to the relevant partial width Γ_j. This procedure makes it possible to treat particle evaporation discretely, and not in the continuous approximation [42,45], and simulates the law of radioactive decay with half-life $\tau_{\rm tot}$. It is important to remark that as the nucleus evaporates particles, the fission probability may change drastically given the change in angular momentum, excitation energy, and fissility. This gives rise to a "natural" interplay between the fission and the ER channel.

The angular momentum L for each Langevin trajectory is sampled by the Monte Carlo method from the spin distribution function [23],

$$\frac{d\sigma(L)}{dL} = \frac{2\pi}{k^2} \frac{2L+1}{1+\exp[(L-L_c)/\delta L]}, \qquad (4)$$

where k, L_c, and δL are the wave number, critical angular momentum for fusion, and diffuseness, respectively. The

TABLE I. The experimental and calculated mean particle multiplicities in the ER and FF channels together with the cross sections.

Viscosity		ER channel			FF channel				
	a	n_{ER}	p_{ER}	α_{ER}	n_{pre}	p_{pre}	α_{pre}	σ_{FF} (mb)	σ_{ER} (mb)
One-body									
$k_s = 0.1$	$A/6$	5.41	1.26	0.55	0.34	0.021	0.013	230	706
$k_s = 0.25$	$A/6$	5.38	1.24	0.54	0.39	0.026	0.016	174	762
$k_s = 0.5$	$A/6$	5.35	1.22	0.54	0.52	0.042	0.017	166	770
$k_s = 1.0$	$A/6$	5.30	1.198	0.56	0.63	0.052	0.030	143	793
$k_s = 1.0$	$A/7$	5.16	1.20	0.61	0.64	0.059	0.041	139	797
$k_s = 1.0$	$A/8$	4.98	1.20	0.70	0.80	0.075	0.061	134	802
Two-body									
$\nu_0 = 0.02$	$A/6$	5.4	1.26	0.52	0.30	0.019	0.009	215	721
$\nu_0 = 0.02$	$A/8$	5.1	1.24	0.66	0.29	0.037	0.022	187	749
$\nu_0 = 0.10$	$A/6$	5.31	1.196	0.56	0.50	0.035	0.022	152	784
$\nu_0 = 0.10$	$A/8$	5.00	1.18	0.69	0.52	0.057	0.041	147	789
$\nu_0 = 0.15$	$A/6$	5.26	1.18	0.57	0.61	0.048	0.028	125	811
$\nu_0 = 0.15$	$A/8$	4.93	1.17	0.71	0.59	0.063	0.043	114	822
$\nu_0 = 0.5$	$A/6$	5.20	1.05	0.60	1.10	0.107	0.089	77	859
$\nu_0 = 0.5$	$A/8$	4.76	1.06	0.76	1.25	0.181	0.174	55	881
Exp.			0.90 ± 0.14	0.56 ± 0.09		0.055 ± 0.007	0.038 ± 0.005	130 ± 13	828 ± 50

values $L_c = 72\hbar$ and $\delta L = 2.5\hbar$ have been estimated from the surface friction model and further constrained to fit the experimental fusion cross section σ_{fus}.

V. RESULTS AND DISCUSSION

Pre-scission light-particle multiplicities are the most sensitive probe for the analysis of the fission dynamics and are widely used to estimate different characteristics like fission time scales and nuclear viscosity. Most of the analysis found in the literature is carried out by using mostly neutron pre-scission multiplicities for cases in which heavy-mass fissioning nuclei are involved. The consideration of systems with intermediate fissility, which have comparable FF and ER cross sections, opens the possibility to study the particle multiplicities and their spectra in both channels. The add on of the ER channel allows us to explore in more detail the slowing down of the fission time scale owing to the nuclear viscosity because this dynamical effect has a consequential impact on the ER cross section and, through the angular momentum and temperature, on the particle multiplicities in the ER channel. The ER channel is therefore able to provide additional constraints in an extended model that includes the dynamical competition between the two channels.

In the fission of the composite system ^{132}Ce the analysis of the data with the statistical model has shown the limitations of a statistical approach [5]. It must be pointed out that this result could be obtained after having measured an extended set of observables, in both ER and FF channels, which strongly constrains the statistical model parameters. In this work, the same observables used in Ref. [5] plus the LCP energy spectra and the MED of fission fragments are compared to the predictions of the dynamical model based on three-dimensional Langevin equations extended to include evaporation of LCPs.

All the observables measured for the reaction 200 MeV $^{32}S + ^{100}Mo$ are presented in the Table I together with the results of a set of dynamical calculations carried out for different values of the dissipation coefficient k_s and level-density parameter a. In the following sections each observable is discussed in detail.

A. FF and ER cross sections and particle multiplicities

The cross sections of FF and ER reaction channels together with the mean multiplicities provide strong constraints on the theoretical model parameters. As one can see from Table I, at fixed viscosity ($k_s = 1$ or $\nu_0 = 0.5$), the decrease of the level-density parameter a from $A/6$ to $A/8$ results in an increase of pre-scission particles multiplicities and decrease of σ_{FF}. In other words, an artificial decrease of a has the same effect as an increase of the viscosity strength. This is an example on how important it is to use an extended set of experimental data to keep parameters under control. Furthermore, the particle multiplicities in the ER channel change as well: n_{ER} decreases, p_{ER} does not change, and α_{ER} increases. This is an angular momentum effect because more energy goes into the collective rotation owing to a reduction of a: The ER cross section is gained at the cost of FF cross section, and this can only occur in the region of higher angular momenta where α particles are more likely to be emitted. The relative change in the competition induced by the angular momentum hinders neutron emission.

The decrease of one-body dissipation coefficient from $k_s = 1.0$ to 0.1 at fixed level-density parameter $a = A/6$ results in a substantial increase of σ_{FF} from 143 to 230 mb. The pre-scission n, p, and α multiplicities decrease two times approximately, when k_s changes from 1.0 to 0.1. This is the expected effect of the nuclear dissipation: To a smaller nuclear dissipation corresponds a larger fission cross section and smaller pre-scission particle multiplicities.

In the case of two-body viscosity the dependence of the observables on the dissipation strength is qualitatively the same as in the case of one-body dissipation. The increase of the viscosity coefficient ν_0 from 0.02×10^{-21} MeV s fm^{-3} to 0.5×10^{-21} MeV s fm^{-3} results in a slight change of multiplicities in ER channels and strong increase of pre-scission particles multiplicities. The $\sigma_{\rm FF}$ values decreases from 215 (187) mb at $\nu_0 = 0.02 \times 10^{-21}$ MeV s fm^{-3} to $\sigma_{\rm FF} = 77$ (55) mb at $\nu_0 = 0.5 \times 10^{-21}$MeV s fm^{-3} and $a = A/6$ ($a = A/8$). Thus, the change of level-density parameter results in a substantial change of predicted multiplicities, as well as $\sigma_{\rm FF}$ and $\sigma_{\rm ER}$ cross sections. At the same time, the change of viscosity coefficient at a fixed a influences the multiplicities in the FF channel and $\sigma_{\rm FF}$ ($\sigma_{\rm ER}$) cross sections only, whereas particle multiplicities in the ER channel change substantially less. The calculations show that to fit experimental data in both ER and FF channels one needs to use level-density parameter $a = A/6$ and strong dissipation $k_s = 1$ (for one-body) or $\nu_0 \simeq 0.15 \times 10^{-21}$ MeV s fm^{-3} (for two-body). In case of low viscosity at fixed level-density parameter the value of $\sigma_{\rm FF}$ is substantially overestimated. For level-density parameter from $A/6$ to $A/8$ the values of $\alpha_{\rm ER}$ are overestimated. Thus, for the best description of experimental data in the case of one-body dissipation one needs to use $k_s = 1$ and $a = A/6$. In these calculations only $p_{\rm ER}$ will be overestimated by approximately 15%.

In the case of two-body dissipation one needs to use $\nu_0 \simeq 0.15 \times 10^{-21}$ MeV s fm^{-3} to get the best description of experimental data. This value is in agreement with previous findings in Ref. [42], where the value $\nu_0 = 0.125 \times 10^{-21}$ MeV s fm^{-3} has been found more suitable for the description of experimental values of $n_{\rm pre}$, as well as $\sigma_{\rm FF}$ and $\sigma_{\rm ER}$. We have to mention here that in Ref. [42] this value of ν_0 is considered to give rise to an unrealistically strong two-body viscosity (close to infinite viscosity) and a smaller fission-fragment kinetic energy. This latter point occurs also in our case study as it is shown later on and constitutes an additional reason why we continue our analysis only with the one-body dissipation model. Furthermore, with $\nu_0 = 0.15 \times 10^{-21}$ MeV s fm^{-3} and $a = A/6$ the calculated $\alpha_{\rm pre}$ value is lower than the experimental one. To improve this discrepancy one can use $a = A/8$. However, the $\alpha_{\rm ER}$ will not be reproduced with this level-density parameter.

Therefore, considering the consistency of our conclusions with the one in Ref. [42] and the analysis of FF and ER cross sections and particle multiplicities, we choose the following model parameters: full ($k_s = 1$) one-body dissipation and $a = A/6$, which provide the best overall description of experimental data presented in Table I. If not specified, later on in the article this basic set of parameters is used for the comparisons between other theoretical calculations and experimental data such as LCP energy spectra and angular correlation ER-LCP.

B. Proton and α-particle energy spectra

Experimental proton and α-particle energy spectra for both ER and FF channels have been compared with the predictions of the dynamical model. Only emission from spherical nuclei has been assumed in the calculation for both

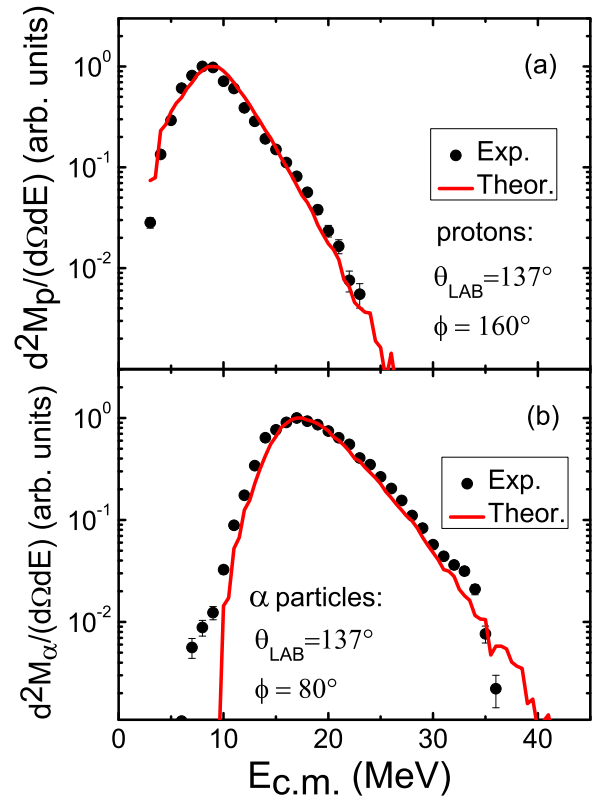

FIG. 3. (Color online) Measured proton (a) and α-particle (b) energy spectra in the center-of-mass system ($\theta_{\rm LAB} = 137°$) for the ER channel compared with the prediction of the dynamical model obtained with the basic set of input model parameters.

channels. We know that this is an important limitation of the actual implementation of the model, and we are working on possible solutions which must take into account the fact that the shape of the fissioning nucleus is known step by step. However, from the comparison with the experimental data we can already infer how important the shape of the nucleus can be in the evaporation process, especially considering that the shape itself is connected with the dissipation strength.

The comparison of the energy spectra for the ER channel is shown in Fig. 3. The good agreement indicates that nearly spherical nuclei are involved in the ER channel. A good agreement is also obtained for α particles in the FF channel (cf. Fig. 4), indicating, also in this case, that these particles are emitted from nearly spherical nuclei. This result implies that pre-scission α particle emission occurs in the early stage of fission, where small deformations are involved. This is in agreement with the findings of Ref. [47], where a phenomenological analysis with the statistical model has been carried out.

As far as pre-scission protons are concerned, the model is not able to reproduce the experimental spectra as well as in the case of the α particles. The excess of measured low-energy protons with respect to the simulation is indicative of strong deformations of the emitter. This deformation should also produce a lowering of the high-energy part of the spectrum, with respect to the spherical case, because of the increase of the

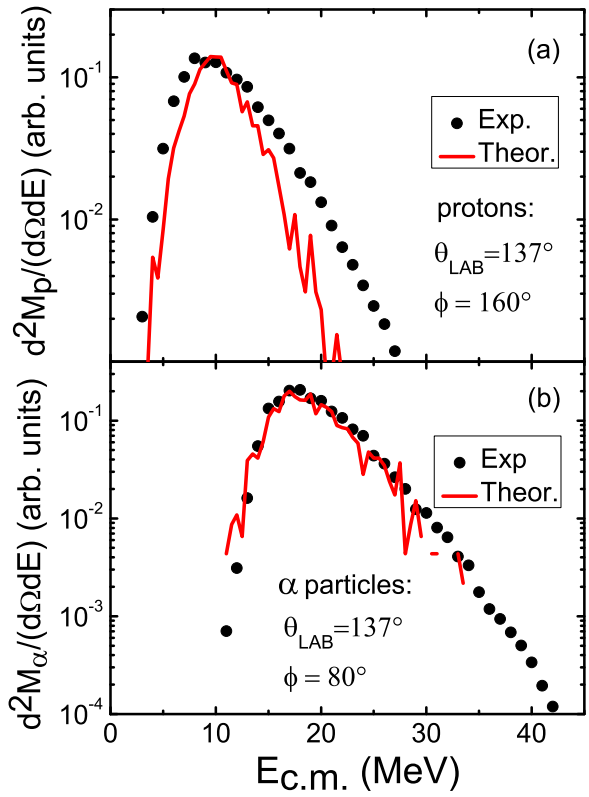

FIG. 4. (Color online) Same as Fig. 3 for the FF channel.

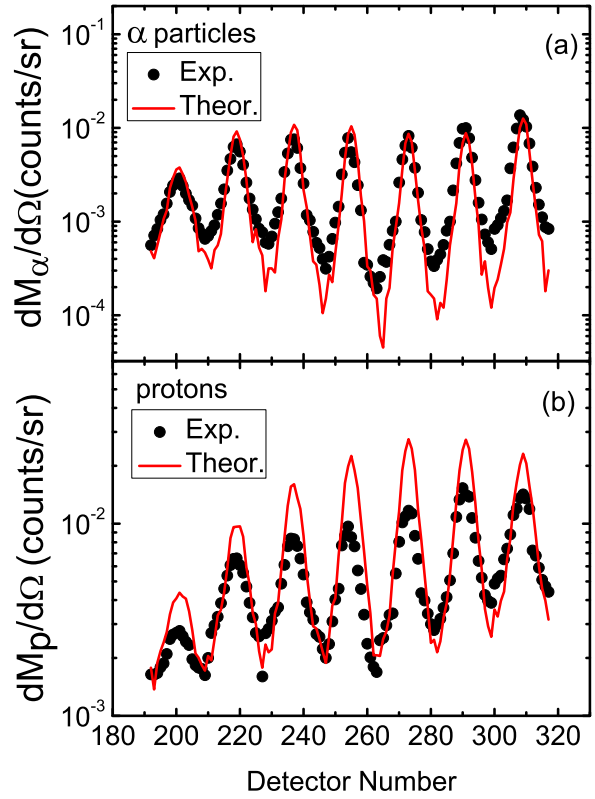

FIG. 5. (Color online) Measured ER-α (a) and ER-p (b) angular correlations, compared with the predictions of the dynamical model. LCP have been detected by $8\pi LP$-BALL detectors, whose number is reported in the abscissa. Evaporation residues have been detected at $\theta_{\rm LAB} = 4.5^{\circ}$.

moment of inertia. This effect, however, is not observed. On the contrary, we observe an excess of high-energy protons with respect to the predictions of the model. The rigorous account of deformation dependence of the statistical model parameters like reduction of emission barriers for charged particles, change of level-density parameter for the deformed shapes of fissioning nucleus, could also change the shape of the spectra. In this respect, the comparison of the data with calculations for deformed nuclei could be particularly elucidating. Such a study will be possible with a further extension of the model, which should include a consistent treatment of particle evaporation taking into account the instantaneous deformation of the compound nucleus determined from the solution of dynamical equations. Nevertheless, the possibility to compute the pre-scission particle energy spectra, even in a simplified way, clearly shows that this additional observable carries valuable information concerning the fission dynamics. A more detailed picture can be achieved when also energy spectra can be reproduced along with the other traditional observables.

C. Angular correlation ER-LCP

The angular correlation between LCPs and ERs is an observable that can be obtained using $8\pi LP$. In fact, owing to the high granularity and the large number of used detectors it is possible to measure the coincidences with a large variety of geometrical configurations. As shown in Fig. 5, the angular distribution has an oscillating behavior as a consequence of a combined effect of kinematics and angular momentum, as shown in Ref. [5]. With reference to the geometry in Fig. 1(b), the maxima correspond to the events where ER and LCP are in plane and on the opposite side of the beam; the minima occur when ER and LCP are in plane and on the same side with respect to the beam direction.

The comparison between calculated and experimental data is shown in Fig. 5. The ER-LCP angular distribution turned out to be more sensitive to the relevant parameters of the statistical model than the spectral shapes. The angular correlation for α particles could be reproduced reasonably well, including the amplitude of the oscillations. The oscillating behavior is reasonably well reproduced also for protons, but mostly the maxima are overestimated by the model. This overestimation reflects the overestimation of $p_{\rm ER}$ reported in Table I. As the values of the model parameters are constrained by the full set of experimental observables, we did not vary them to improve the agreement only for ER-proton angular correlation. A better agreement could indeed be obtained by changing the parameters of the statistical model which could decrease the $p_{\rm ER}$ value [5], but this would have contradicted the approach of this work.

D. Mass-energy distribution of fission fragments

Figure 6(a) shows the MED as measured and Fig. 6(b) shows the MED computed with the dynamical model and the basic set of parameters. One can see a qualitative agreement in

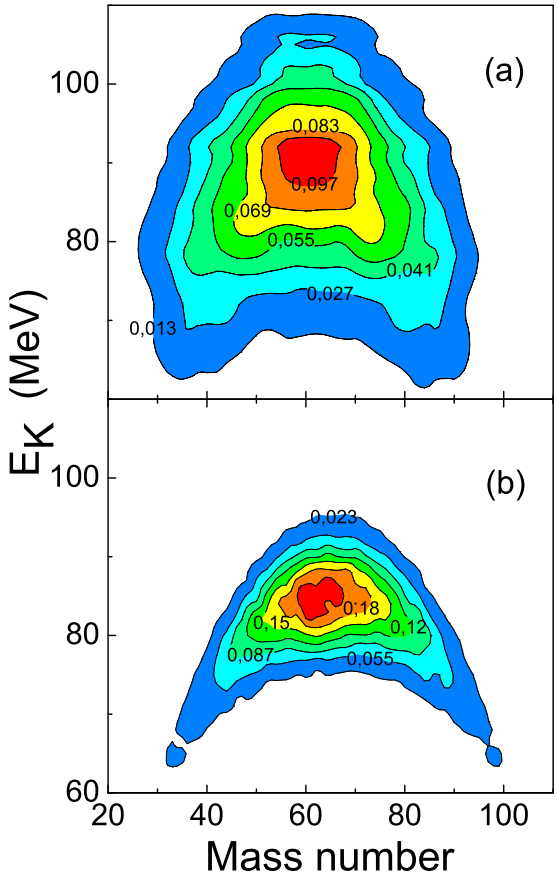

FIG. 6. (Color online) Experimental (a) and theoretical (b) MED of fission fragments for the ^{132}Ce composite system. See text for details.

the general behavior of the contours between the experimental and theoretical two-dimensional plots. However, the calculated distribution deviates from the experimental one in the energy range around the symmetric fission. In the calculations there are no events with $E_K > 95$ MeV and $E_K < 75$ MeV at nearly symmetric fission. This indicates that in the dynamical calculations, at the scission point, the parametric geometrical representation chosen for the shapes is not suitable to sample a sufficiently large variety of shapes of the fissioning nuclei. In particular, there is not enough variability in the elongation of the scission configurations for a given mass asymmetry. Introducing a more flexible shape parametrization at the scission region could generate a larger variety of E_K values, with the result of expanding calculated MED with respect to the E_K axis.

E. Total kinetic-energy distribution of fission fragments

The kinetic-energy distribution of fission fragments is obtained by integration of two-dimensional MED over fission-fragment mass. The comparison between calculated and experimental kinetic-energy distribution of fission fragments is presented in Fig. 7, where the difference between them is clearly seen. The yield of calculated energy distribution is substantially lower than the experimental one in the range of

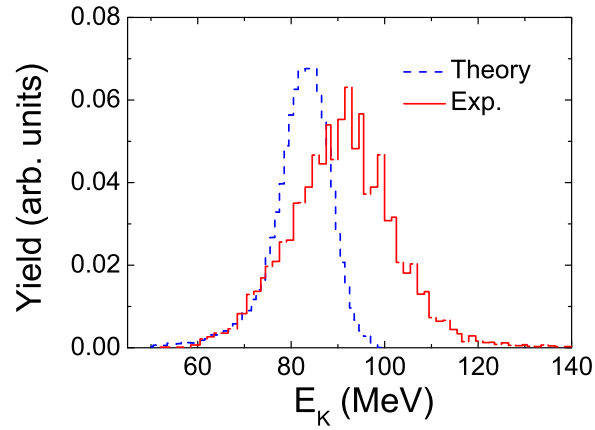

FIG. 7. (Color online) Experimental and theoretical kinetic-energy distribution of fission fragments.

high E_K values: 95 MeV $< E_K <$ 120 MeV, the latter being substantially wider than the calculated one. A similar result has been obtained in three-dimensional Langevin calculations in Refs. [13,39,48]. The maxima of kinetic-energy distributions show a difference of about 10 MeV.

To get a better reproduction of the experimental kinetic-energy distribution, one needs to use lower values of viscosity $k_s \simeq 0.1$–0.25, which does not make it possible to reproduce the pre-scission particle multiplicities [49]. Furthermore, the sensitivity of the standard deviation of the energy distribution σ_{E_K} to k_s is very small, as shown in Table II, where calculated parameters of MED for different sets of input parameters are presented. As can be seen from Table II, the increase of σ_{E_K} from 7.3 to 8.1 MeV is obtained for $a = A/6$ for one-body

TABLE II. Experimental and calculated parameters of fission-fragment MED. σ_M and σ_{E_K} are the standard deviation of the mass and energy distribution, respectively. $\langle E_K \rangle$ is the average value of the energy distribution. The experimental value of $\langle E_K \rangle = 85.9$ MeV has been estimated from Viola's systematics [50].

Viscosity	a	σ_M (a.m.u.)	σ_{E_K} (MeV)	$\langle E_K \rangle$ (MeV)
One-body				
$k_s = 0.1$	$A/6$	16.3	8.1	82.6
$k_s = 0.25$	$A/6$	16.0	7.7	82.5
$k_s = 0.5$	$A/6$	15.5	7.6	82.2
$k_s = 1.0$	$A/6$	14.9	7.3	82.0
$k_s = 1.0$	$A/7$	16.2	8.3	81.7
$k_s = 1.0$	$A/8$	16.4	8.4	80.9
Two-body				
$\nu_0 = 0.02$	$A/6$	15.2	7.6	81.9
$\nu_0 = 0.10$	$A/6$	15.1	7.5	79.6
$\nu_0 = 0.15$	$A/6$	14.6	6.7	79.6
$\nu_0 = 0.5$	$A/6$	14.2	6.6	78.6
$\nu_0 = 0.02$	$A/8$	16.6	8.5	81.3
$\nu_0 = 0.10$	$A/8$	16.3	8.4	78.8
$\nu_0 = 0.15$	$A/8$	16.1	8.1	78.6
$\nu_0 = 0.5$	$A/8$	14.9	7.0	78.4
Exp.		15.4	11.4	90.9 (85.9)

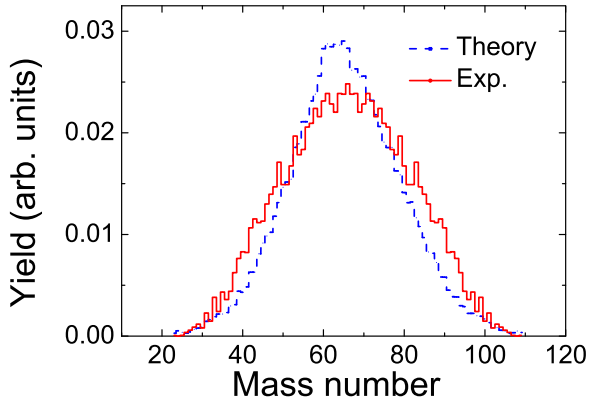

FIG. 8. (Color online) Experimental and theoretical mass distributions of fission fragments.

dissipation going from $k_s = 1$ to $k_s = 0.1$. The increase of the level-density parameter a produces a slight increase of σ_{E_k} as well. Concerning two-body dissipation we obtain similar qualitative behavior of σ_{E_k} with change of viscosity and level-density parameter.

In dynamical simulations the kinetic energies of fission fragments are determined at the moment of scission and depend on the scission criterion used in the calculations. The investigation of the influence of different scission criteria on the energy distribution is presented in Ref. [48]. In this paper it was shown that commonly accepted scission criteria in nuclear physics could not provide a reasonable description of experimental energy distribution for fissioning nuclei in a large range of Z^2/A in the calculations based on the (c,h,α) parametrization. This parametrization does not provide sufficient variability of the nuclear shapes at the scission region [48] because it uses only one parameter to govern the neck size. The parameter (h) governs the neck thickness but not its length. A possible way to improve the theoretical description of the experimental data on kinetic-energy distribution could be to use another parametrization, which could provide more flexible shapes of the compound nucleus during the descent from saddle to scission, with independent shape parameters [51–53] determining the length of the neck and its thickness.

F. Mass distribution of fission fragments

The mass distribution of fission fragments is presented in Fig. 8. One can see that the theoretical calculations with one-body dissipation is able to reproduce reasonably well the experimental data, although the model slightly underestimates the width of the distribution. To improve the description of experimental mass distribution, one can use lower values of k_s. In this case the variance of mass distribution becomes larger or, in other words, the calculated mass distribution becomes wider. However, the pre-scission particle multiplicities will not be reproduced in this case. The variances of mass and TKE distributions for ^{132}Ce are not very sensitive to nuclear dissipation, as shown in Table II. The variances change only about 25% when the viscosity coefficient k_s changes from 0.1 to 1. This feature of mass distribution is attributable to a

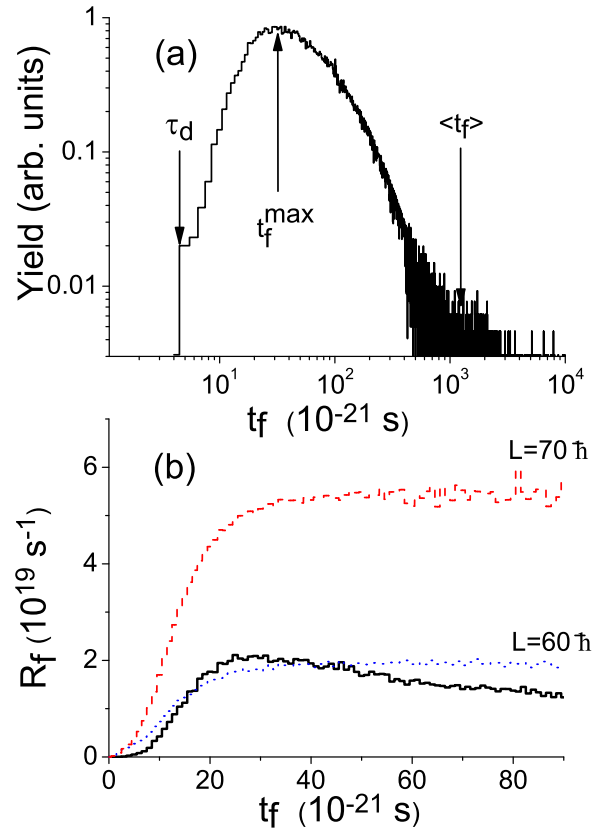

FIG. 9. (Color online) (a) Fission time distribution; (b) fission rate obtained in the calculations with the dynamical model. In (b), dashed and dotted lines refer to calculations without particle evaporations. See text for details.

short descent from the saddle to the scission point for light nuclei. The fissioning system ^{132}Ce passes the region between saddle and scission point in approximately 3×10^{-21} s. Moreover, the stiffness of potential energy with respect to the mass-asymmetry coordinate at saddle and scission points is approximately the same. Therefore, during the descent from the saddle to the scission point the fluctuations of mass-asymmetry collective coordinates, which determine the width of mass distribution, have not the opportunity to become large.

G. Fission time scale

The analysis of the fission time scale is important for understanding the dynamics, as one can explore the influence of the many ingredients of the model at different stages of the fission process. From the dynamical model and the computational method it is possible to build the time distribution of all fission events. The fission time distribution for ^{132}Ce composite system predicted by the dynamical model, anchored on the full set of experimental data, is presented in Fig. 9(a) together with the fission rate R_f for the case of one-body dissipation with $k_s = 1$ and $a = A/6$.

This figure reveals indeed that fission can take place in quite a broad interval of time. In the time interval $0 < t < \tau_d$ there are no fission events at all. The time $\tau_d = 5 \times 10^{-21}$ s

TABLE III. The parameters of fission time distribution extracted from the simulation with the dynamical model.

Compound system	τ_d 10^{-21} s	$t_f^{\max}$ 10^{-21} s	$\langle t_f \rangle$ 10^{-21} s
^{132}Ce	5	30	1250

could be considered the analog of the delay parameter often used in fission studies [23,54]. Furthermore, we observe a steep rise from $\tau_d = 5 \times 10^{-21}$ s up to the maximum at $t = t_f^{\max} \simeq 30 \times 10^{-21}$ s. At $t > t_f^{\max}$ the fission time distribution has a nearly exponential decrease with a long tail lasting up to 10^{-18} s. The arrow at $t = 1250 \times 10^{-21}$ s indicates the mean fission time $\langle t_f \rangle$. This value is strongly influenced by the tail of the fission time distribution. The parameters that characterize this fission time distribution are reported in Table III. They are obtained from the calculation that provides the best description of the experimental data in ER and FF channels.

In Fig. 9(b) the fission rate $R_f(t)$ obtained in the same calculation is presented. The fission rate calculated at fixed angular momenta $L = 60\hbar$ and $70\hbar$ of the initial compound nucleus, without including evaporation along the trajectories, shows sensitivity of $R_f(t)$ to angular momentum. As expected, the relative probability of fissioning increases with the angular momentum. The trend of the fission rate which includes particle evaporation and all the angular momenta distributed according to Eq. (4) (solid line) demonstrates the strong influence of particle evaporation on the fission rate. The $R_f(t)$ functions at $L = 60\hbar$ $[R_f^*(L = 60\hbar, t)]$ and $70\hbar$ $[R_f^*(L = 70\hbar, t)]$ represent approximate limits (in case of no evaporation), as L values of $60\hbar$ and $70\hbar$ correspond to the sharp cutoff values for the FF cross section. Inclusion of evaporation in the calculation results in a substantial decrease of E_x from the beginning of the decay process. As a result, the realistic $R_f(t)$ just slightly overcomes the limiting value $R_f^*(L = 60\hbar, t)$ at $t \simeq 30 \times 10^{-21}$ s and after has a smooth decrease.

From the comparison between the $R_f(t)$ and the fission time distribution one can see a straight correlation in the behavior between these two quantities. The fission delay time τ_d is equal to 5×10^{-21} s and $R_f(t < \tau_d) = 0$, which means that no fission events occur before τ_d. The steep rise of fission time distribution corresponds to the increase of $R_f(t)$ until the maximum value. The maxima of $R_f(t)$ and fission time distribution are at $t_f^{\max} \simeq 30 \times 10^{-21}$ s. For $t > t_f^{\max}$ the smooth decrease of $R_f(t)$ corresponds to the nearly exponential decrease of fission time distribution.

To illustrate how particle evaporation is distributed in time before fission occurs, we show in Fig. 10(a) the percentage yields of the first- $[Y_{n1}(t)]$, the second- $[Y_{n2}(t)]$, and the third-chance $[Y_{n3}(t)]$ pre-scission neutron as a function of time. The yields for the first-chance pre-scission proton and α particle are presented in Fig. 10(b). From these figures one can see that particle evaporation starts from $t = 0$. The yields for the first-chance neutron, proton, and α particle have approximately the same behavior as a function of time. It is an exponential decrease from the maximum at $t = 0$ to zero at $t = 250 \times 10^{-21}$ s. Considering the multiple emission of

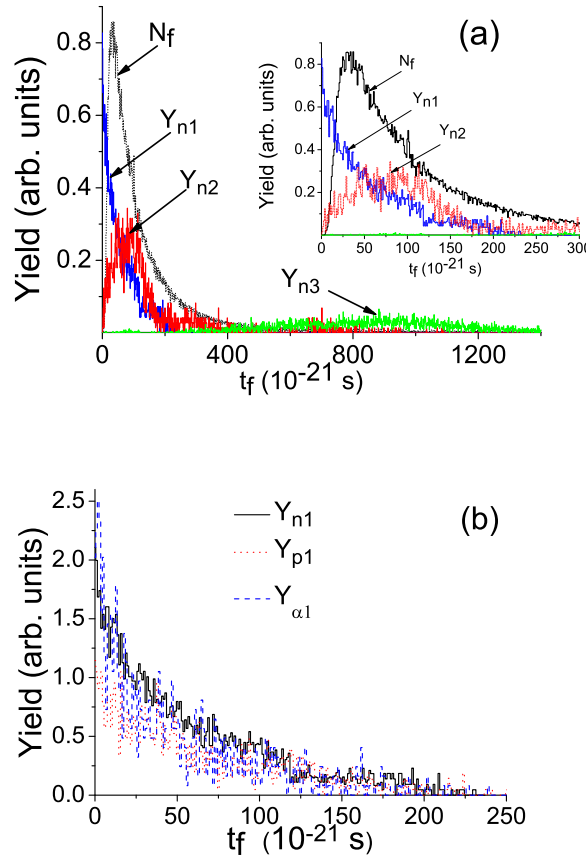

FIG. 10. (Color online) Distribution of the yields of pre-scission particle multiplicities vs time of emission from equilibrium: (a) first- (Y_{n1}), second- (Y_{n2}), and third- (Y_{n3}) chance pre-scission neutrons together with time distribution of fission events (N_f); (b) first-chance neutron (Y_{n1}), proton (Y_{p1}) and α particle ($Y_{\alpha 1}$). See text for details.

neutrons, one can see that the emission of every further neutron requires a correspondingly larger time. The maxima for $Y_{2n}(t)$ and $Y_{3n}(t)$ are at nearly 100×10^{-21} s and 900×10^{-21} s, respectively. The main reason for such a behavior is the reduction of the excitation energy E_x after each evaporation step.

From the investigation of the characteristic times of particle emissions one can estimate the time scales of the different steps accompanying the decay of the compound nucleus. Clearly, the calculation of the time distribution in our dynamical model can provide a key to an explanation of why, in the statistical model approach to fission dynamics, broad and controversial values of characteristic fission delays or viscosity coefficients are found in the literature using different probes and different reactions [9]. Our work can open an important discussion on this point that will be the subject of a forthcoming article. The conclusions of this study are that our extensive set of data is consistent with a deformation-dependent one-body viscosity model and that after a time $\tau_d = 5 \times 10^{-21}$ s, fission occurs in an interval of time that can cover four orders of magnitude. To give more strength to the above conclusions and the methodology used in this work, the measurement of the neutron multiplicities in the FF and ER channels would be remarkably important and has been planned.

VI. SUMMARY AND CONCLUSIONS

The fission dynamics for the composite system ^{132}Ce at excitation energy $E_x = 122$ MeV, has been studied experimentally and theoretically. Experiments were carried out at the LNL to measure LCP multiplicities and energy spectra in the FF and ER channels, as well as channel cross sections, ER-LCP correlations, and MED of fission fragments. Data have been analyzed in the framework of a dynamical model based on three-dimensional Langevin equations.

By using the dynamical model, most of the observables are reproduced assuming full one-body dissipation with reduction factor from the contribution from the wall formula $k_s = 1$. This type of dissipation leads to a strongly shape-dependent reduced viscosity parameter $\beta_{q_2q_2}$ responsible for the dynamical evolution of decaying system to fission direction. In particular, the fission proceeds with large values of $\beta_{q_2q_2} \simeq 24 \times 10^{21}$ s^{-1} for nearly spherical shapes at the beginning of the process, with a decreasing behavior of $\beta_{q_2q_2}$ reaching the value $\beta_{q_2q_2} \simeq 5 \times 10^{21}$ s^{-1} for highly deformed shapes. A good agreement between theoretical calculations and experimental data on cross sections $\sigma_{\rm FF}$ and $\sigma_{\rm ER}$ and particle multiplicities in ER and FF channels have been obtained at $k_s = 1$ ($a = A/6$) for the case of one-body dissipation and $\nu_0 = 0.15$ MeV s fm^{-3} ($a \simeq A/7$) for two-body dissipation.

The fission-fragment mass distribution is reasonably well reproduced by the dynamical model, as well as the average kinetic energy of fission fragments, while the width of fission-fragment kinetic-energy distribution is underestimated. This failure is related to the limited types of nuclear shapes generated by the (c,h,α) parametrization for the scission configurations [48]. The best agreement between calculated MED and experimental data has been obtained with full one-body dissipation $k_s = 1$ and level-density parameter $a = A/6$. An agreement of same quality with data is also obtained assuming an unusually large value of two-body friction, $\nu_0 = 0.15 \times 10^{-21}$ MeV s fm^{-3}, which corresponds to the $\beta_{q_2q_2} \simeq 50 \times 10^{21}$ s^{-1} for nearly spherical shape and smooth decrease to the $\beta_{q_2q_2} \simeq 25 \times 10^{21}$ s^{-1} at scission. However, the mean kinetic energy $\langle E_K \rangle$ is better reproduced in the calculations with one-body dissipation than in the calculations with the two-body dissipation. The $\langle E_K \rangle$ values obtained in the calculations with two-body viscosity are lower than the experimental one. This result is in agreement with the previous findings [42]. The large inconsistency of the friction coefficient of two-body dissipation $\nu_0 = 0.15 \times 10^{-21}$ MeV s fm^{-3} with previous findings [40,41] and the worse description of $\langle E_K \rangle$ brings us to exclude this mechanism as dominant in the fission of the studied system. In the present calculations we did not consider any temperature dependence of dissipation.

The fission time distribution provided by the dynamical model with full one-body dissipation has the following characteristics: mean fission time $\langle t_f \rangle = 1250 \times 10^{-21}$ s, delay time $\tau_d = 5 \times 10^{-21}$ s, and time needed to build up the maximum value of the fission rate $\tau_f^{\rm max} \simeq 30 \times 10^{-21}$ s.

The pre-scission α-particle energy spectra are consistent with emission from spherical nuclei, indicating that these particles are evaporated in the early stage of the fission process, where small deformations are involved. Similar results have been reported in Ref. [47]. Concerning pre-scission proton spectra, the excess of low-energy particles with respect to the prediction of the model is indicative of strong emitter deformations. This result leaves an open question and stimulates a further development of the theoretical model which should use the deformation-dependent statistical-model parameters to treat evaporation from deformed shapes of fissioning nucleus.

ACKNOWLEDGMENTS

The author wish to thank the staff at LNL for the excellent support in carrying out these experiments. One of us (P.N.N.) is grateful to the Istituto Nazionale di Fisica Nucleare (INFN) for financing his stay in Naples and also wishes to thank the Naples section of INFN for the warm hospitality. This study was partially supported by the Russian Foundation for Basic Research, Research Project No. 13-02-00168 (Russia).

[1] D. Hilscher and H. Rossner, Ann. Phys. (Paris) **17**, 471 (1992).
[2] D. J. Hinde, D. Hilscher, H. Rossner, B. Gebauer, M. Lehmann, and M. Wilpert, Phys. Rev. C **45**, 1229 (1992).
[3] J. P. Lestone, J. R. Leigh, J. O. Newton, D. J. Hinde, J. X. Wei, J. X. Chen, S. Elfström, and M. Zielinska-Pfabé, Nucl. Phys. A **559**, 277 (1993).
[4] E. Vardaci *et al.*, Eur. Phys. J. A **43**, 127 (2010).
[5] A. Di Nitto *et al.*, Eur. Phys. J. A **47**, 83 (2011).
[6] T. Wada, N. Carjan, and Y. Abe, Nucl. Phys. A **538**, 283 (1992).
[7] P. N. Nadtochy, A. Kelić, and K.-H. Schmidt, Phys. Rev. C **75**, 064614 (2007).
[8] E. Vardaci *et al.*, in *Proceedings of the 4th International Conference on Dynamical Aspects of Nuclear Fission, Častá–Papiernička, Slovak Republic, October 19–23, 1998*, edited by Yu. Ts. Oganessian, J. Kliman, and Š. Gmuca (World Scientific, Singapore, 2000), pp. 261–272.
[9] E. Vardaci *et al.*, in *Proceedings of the 6th International Conference on Dynamics Aspects of Nuclear Fission, Smolenice Castle, Slovak Republic, October 2–6, 2006*, edited by J. Kliman, M. G. Itkis, and Š. Gmuca (World Scientific, Singapore, 2008), pp. 8–21, and references therein.
[10] L. Fiore *et al.*, Nucl. Phys. A **620**, 71 (1997).
[11] R. Moro *et al.*, Eur. Phys. J. A **48**, 159 (2012).
[12] G. La Rana *et al.*, Eur. Phys. J. A **16**, 199 (2003).
[13] A. V. Karpov, P. N. Nadtochy, D. V. Vanin, and G. D. Adeev, Phys. Rev. C **63**, 054610 (2001).
[14] P. N. Nadtochy, G. D. Adeev, and A. V. Karpov, Phys. Rev. C **65**, 064615 (2002).
[15] E. G. Ryabov, A. V. Karpov, P. N. Nadtochy, and G. D. Adeev, Phys. Rev. C **78**, 044614 (2008).
[16] E. Fioretto *et al.*, IEEE Trans. Nucl. Sci. **44**, 1017 (1997).
[17] S. Beghini, C. Signorini, S. Lunardi, M. Morando, G. Fortuna, A. M. Stefanini, W. Meczynski, and R. Pengo, Nucl. Instrum. Methods Phys. Res. A **239**, 585 (1985).
[18] E. Kozulin, A. A. Bogachev, M. G. Itkis, I. M. Itkis, G. N. Knyazheva, N. A. Kondratiev, L. Krupa, I. V. Pokrovsky, and E. V. Prokhorova, Instrum. Exp. Tech. **51**, 44 (2008).
[19] M. G. Itkis and A. Ya. Rusanov, Phys. Part. Nucl. **29**, 160 (1998).

[20] M. Brack, J. Damgaard, A. S. Jensen, H. C. Pauli, V. M. Strutinsky, and C. Y. Wong, Rev. Mod. Phys. **44**, 320 (1972).
[21] H. A. Kramers, Physica **7**, 284 (1940).
[22] Y. Abe, S. Ayik, P.-G. Reinhard, and E. Suraud, Phys. Rep. **275**, 49 (1996).
[23] P. Fröbrich and I. I. Gontchar, Phys. Rep. **292**, 131 (1998).
[24] V. Zagrebaev and W. Greiner, in *Cluster in Nuclei*, edited by C. Beck (Springer-Verlag, Berlin, Heidelberg, 2010), Vol. 1; V. Zagrebaev and W. Greiner, Lect. Notes Phys. **818**, 267 (2010).
[25] G. D. Adeev, A. V. Karpov, P. N. Nadtochii, and D. Vanin, Phys. Part. Nucl. **36**, 378 (2005) [Fiz. Elem. Chastits At. Yadra **36**, 732 (2005)].
[26] P. N. Nadtochy and G. D. Adeev, Phys. Rev. C **72**, 054608 (2005).
[27] K. T. R. Davies, A. J. Sierk, and J. R. Nix, Phys. Rev. C **13**, 2385 (1976).
[28] H. J. Krappe, J. R. Nix, and A. J. Sierk, Phys. Rev. C **20**, 992 (1979).
[29] A. J. Sierk, Phys. Rev. C **33**, 2039 (1986).
[30] J. Blocki, Y. Boneh, J. Nix, J. Randrup, M. Robel, A. J. Sierk, and W. J. Swiatecki, Ann. Phys. (NY) **113**, 330 (1978).
[31] J. Randrup and W. J. Swiatecki, Ann. Phys. (NY) **125**, 193 (1980).
[32] J. R. Nix and A. J. Sierk, in *Proceedings of the International School-Seminar on Heavy Ion Physics, Dubna, USSR, 1986*, edited by M. I. Zarubina and E. V. Ivashkevich (JINR, Dubna, 1987), pp. 453–464.
[33] J. R. Nix and A. J. Sierk, in *Proceedings of the 6th Adriatic Conference on Nuclear Physics: Frontiers of Heavy Ion Physics, Dubrovnik, Yugoslavia, 1987*, edited by N. Cindro, R. Caplar, and W. Greiner (World Scientific, Singapore, 1990), pp. 333–340.
[34] J. J. Griffin and M. Dworzecka, Nucl. Phys. A **455**, 61 (1986).
[35] S. Pal and T. Mukhopadhyay, Phys. Rev. C **54**, 1333 (1996).
[36] T. Mukhopadhyay and S. Pal, Phys. Rev. C **56**, 296 (1997).
[37] S. Pal and T. Mukhopadhyay, Phys. Rev. C **57**, 210 (1998).
[38] H. Feldmeier, Rep. Prog. Phys. **50**, 915 (1987).
[39] P. N. Nadtochy, A. V. Karpov, and G. D. Adeev, Phys. At. Nucl. **65**, 799 (2002).
[40] A. J. Sierk and J. R. Nix, Phys. Rev. C **21**, 982 (1980).
[41] J. R. Nix and A. J. Sierk, Nucl. Phys. A **428**, 161 (1984).
[42] T. Wada, Y. Abe, and N. Carjan, Phys. Rev. Lett. **70**, 3538 (1993).
[43] LILITA program was written by J. Gomez del Campo and R. G. Stockstad, Oak Ridge National Laboratory Report No. TM7295, 1981.
[44] L. C. Vaz and J. M. Alexander, Z. Phys. A **318**, 231 (1984).
[45] G. R. Tillack, Phys. Lett. B **278**, 403 (1992).
[46] N. D. Mavlitov, P. Fröbrich, and I. I. Gontchar, Z. Phys. A **342**, 195 (1992).
[47] H. Ikezoe *et al.*, Phys. Rev. C **46**, 1922 (1992).
[48] M. V. Borunov, P. N. Nadtochy, and G. D. Adeev, Nucl. Phys. A **799**, 56 (2008).
[49] P. N. Nadtochy, A. V. Karpov, D. V. Vanin, and G. D. Adeev, Phys. At. Nucl. **66**, 1203 (2003).
[50] V. E. Viola, K. Kwiatkowski, and M. Walker, Phys. Rev. C **31**, 1550 (1985).
[51] P. Möller, A. J. Sierk, T. Ichikawa, A. Iwamoto, R. Bengtsson, H. Uhrenholt, and S. Åberg, Phys. Rev. C **79**, 064304 (2009).
[52] J. Randrup and P. Möller, Phys. Rev. Lett. **106**, 132503 (2011).
[53] V. Pashkevich and A. Rusanov, Nucl. Phys. A **810**, 77 (2008).
[54] P. Grange, Li Jun-Qing, and H. A. Weidenmuller, Phys. Rev. C **27**, 2063 (1983).